Probing Decoherence with Electromagnetically Induced Transparency in Superconductive Quantum Circuits

K. V. R. M. Murali,[1] Z. Dutton,[2] W. D. Oliver,[3] D. S. Crankshaw,[1] and T. P. Orlando[1]

[1]*Department of Electrical Engineering and Computer Science, Massachusetts Institute of Technology, Cambridge, Massachusetts 02139, USA*

[2]*Electron and Optical Division, National Institute of Standards & Technology, Gaithersburg Maryland 20899-8410, USA*

[3]*MIT Lincoln Laboratory, 244 Wood Street, Lexington, Massachusetts 02420, USA*

(Received 20 November 2003; published 17 August 2004)

Superconductive quantum circuits comprise quantized energy levels that may be coupled via microwave electromagnetic fields. Described in this way, one may draw a close analogy to atoms with internal (electronic) levels coupled by laser light fields. In this Letter, we present a superconductive analog to electromagnetically induced transparency that utilizes superconductive quantum circuit designs of present day experimental consideration. We discuss how a superconductive analog to electromagnetically induced transparency can be used to establish macroscopic coherence in such systems and, thereby, be utilized as a sensitive probe of decoherence.

DOI: 10.1103/PhysRevLett.93.087003 PACS numbers: 85.25.–j, 03.67.–a, 42.50.Gy

Superconductive quantum circuits (SQCs) comprising mesoscopic Josephson junctions can exhibit quantum coherence among their macroscopically large degrees of freedom [1]. They feature quantized flux and/or charge states depending on their fabrication parameters, and the resultant quantized energy levels are analogous to the quantized internal levels of an atom. Spectroscopy, Rabi oscillation, and Ramsey interferometry experiments have demonstrated that SQCs behave as "artificial atoms" under carefully controlled conditions [2–8]. This Letter extends the SQC-atom analogy to another quantum optical effect associated with atoms: electromagnetically induced transparency (EIT) [9,10]. We propose the demonstration of microwave transparency using a superconductive analog to EIT (denoted S-EIT) in a superconductive circuit exhibiting two metastable states (e.g., a qubit) and a third, shorter-lived state (e.g., the readout state). We show that driving coherent microwave transitions between the qubit states and the readout state is a demonstration of S-EIT. We further propose a means to use S-EIT to probe sensitively the qubit decoherence rate; the philosophy is similar to proposed EIT-based measurements of phase diffusion in atomic Bose-Einstein condensates [11].

The three-level Λ system illustrated in Fig. 1(a) is a standard energy level configuration utilized in EIT [9,10]. It comprises two metastable states $|1\rangle$ and $|2\rangle$, each of which may be coupled to a third excited state $|3\rangle$. In atoms, the metastable states are typically hyperfine or Zeeman levels, while state $|3\rangle$ is an excited electronic state that may spontaneously decay at a relatively fast rate Γ_3. In an atomic EIT scheme, a resonant "probe" laser couples the $|1\rangle \leftrightarrow |3\rangle$ transition, and a "control" laser couples the $|2\rangle \leftrightarrow |3\rangle$ transition. The transition coupling strengths are characterized by their Rabi frequencies $\Omega_{j3} \equiv -\mathbf{d}_{j3} \cdot \mathbf{E}_{j3}$ for $j = 1, 2$, respectively, where $\mathbf{d}_{j3}$ are the dipole matrix elements and $\mathbf{E}_{j3}$ are the slowly varying envelopes of the electric fields. For particular Rabi frequencies Ω_{j3}, the probe and control fields are effectively decoupled from the atoms by a destructive quantum interference of the two driven transitions. The result is probe and control field transparency [9,10]. In recent experiments, ultraslow light propagation due to EIT-based refractive-index modifications in atomic clouds has been observed [15–17].

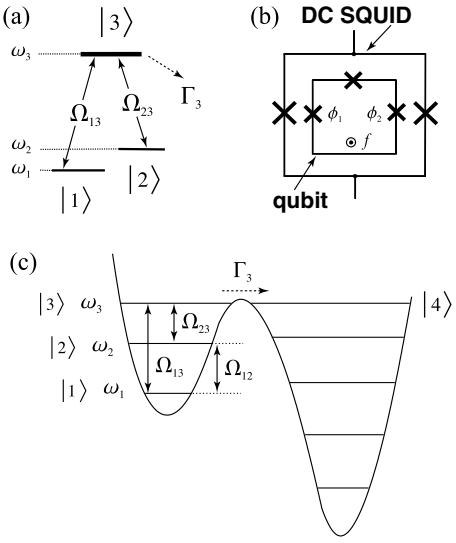

FIG. 1. (a) Energy level diagram of a three-level Λ system. EIT can occur in atoms possessing two long-lived states $|1\rangle$, $|2\rangle$, each of which is coupled via resonant laser light fields to a radiatively decaying state $|3\rangle$. (b) Circuit schematic of the persistent-current (PC) qubit and its readout SQUID. (c) One-dimensional double-well potential and energy-level diagram for a three-level SQC. Using PC qubit parameters [12–14], we calculate $\omega_2 - \omega_1 = (2\pi)$ 36 GHz and $\omega_3 - \omega_2 = (2\pi)$ 32 GHz. The simulated matrix elements $\langle p|\sin(2\pi f + 2\phi_m)|q\rangle$ for $(p, q) = (1, 2)$, $(2, 3)$, and $(1, 3)$ are, respectively, 0.0704, -0.125, and 0.0158.

 0031-9007/04/93(8)/087003(4)$22.50 © 2004 The American Physical Society

SQCs also exhibit Λ-like energy level structures [7,12,13,18–21]. One example is the PC qubit, a superconductive loop interrupted by two Josephson junctions of equal size and a third junction scaled smaller in area by the factor $\alpha < 1$ [Fig. 1(b)] [14,22]. Its dynamics are described by the Hamiltonian

$$\mathcal{H}_{\mathrm{PC}} = \frac{1}{2}C\left(\frac{\Phi_0}{2\pi}\right)^2[\dot{\varphi}_p^2 + (1+2\alpha)\dot{\varphi}_m^2] + E_J[2+\alpha-2\cos\varphi_p\cos\varphi_m - \alpha\cos(2\pi f + 2\varphi_m)], \quad (1)$$

in which C is the capacitance of the larger junctions, $\varphi_{p,m} \equiv (\varphi_1 \pm \varphi_2)/2$, φ_i is the gauge-invariant phase across the larger junctions $i = \{1, 2\}$, E_J is the Josephson coupling energy, and f is the magnetic flux through the loop in units of the flux quantum Φ_0 [14]. Near $f \approx 1/2$, the qubit potential landscape [second term in Eq. (1)] assumes a double-well profile. Each well corresponds to a distinct classical state of the electric current, i.e., left or right circulation about the qubit loop, and its net magnetization is discernible using a dc SQUID [14]. As a quantum object, the potential wells exhibit quantized energy levels corresponding to the quantum states of the macroscopic circulating current [13,18]. These levels may be coupled using microwave radiation [4,12], and their quantum coherence has been experimentally demonstrated [8].

Tuning the flux bias away from $f = 1/2$ results in the asymmetric double-well potential illustrated in Fig. 1(c). The three states in the left well constitute the superconductive analog to the atomic Λ system. Using tight-binding models with experimental PC qubit parameters [12–14] at a flux bias $f = 0.5041$, we estimate the interwell resonant-tunneling rates for states $|1\rangle$, $|2\rangle$, and $|3\rangle$ to be $\Gamma_1^{(\mathrm{rt})} \approx (1\ \mathrm{ms})^{-1}$, $\Gamma_2^{(\mathrm{rt})} \approx (1\ \mu\mathrm{s})^{-1}$, and $\Gamma_3^{(\mathrm{rt})} \approx (1\ \mathrm{ns})^{-1}$, respectively. An off-resonant biasing of state $|3\rangle$ decreases its interwell tunneling rate to order $(100\ \mu\mathrm{s})^{-1}$ [23]; the off-resonant biasing of states $|1\rangle$ and $|2\rangle$ [as in Fig. 1(c)] will also significantly decrease their interwell tunneling rates. In addition, the intrawell relaxation rate at a similar flux bias was experimentally determined to be $\Gamma_3^{(\mathrm{intra})} \approx (25\ \mu\mathrm{s})^{-1}$ [12] and, presumably, $\Gamma_2^{(\mathrm{intra})} < \Gamma_3^{(\mathrm{intra})}$. Therefore, the "qubit states" $|1\rangle$ and $|2\rangle$ are effectively metastable with respect to the resonantly biased "readout state" $|3\rangle$. Since $\Gamma_3^{(\mathrm{rt})} \gg \Gamma_3^{(\mathrm{intra})}$ [12,13,18], a particle reaching state $|3\rangle$ will tunnel quickly to state $|4\rangle$, an event that is detectable by a dc SQUID. Alternatively, for slower detection schemes, one may detune states $|3\rangle$ and $|4\rangle$ and then apply a resonant π pulse to transfer the population from state $|3\rangle$ to $|4\rangle$.

Transitions between the quantized levels are driven by resonant microwave-frequency magnetic fields. Assuming the Rabi frequencies Ω_{ij} to be much smaller than all level spacings $|\omega_{kl}| \equiv |\omega_k - \omega_l|$, the system-field interaction may be written within the rotating wave approximation (RWA) [24],

$$\mathcal{H}_{\mathrm{int}}^{(\mathrm{RWA})} = \frac{\hbar}{2}\begin{bmatrix} 0 & \Omega_{12}^* & \Omega_{13}^* \\ \Omega_{12} & 0 & \Omega_{23}^* \\ \Omega_{13} & \Omega_{23} & -i\Gamma_3 \end{bmatrix}, \quad (2)$$

in which the decay from state $|3\rangle$ is treated phenomenologically as a non-Hermitian matrix element [24,25]. For small microwave perturbations of the frustration, Δf, the associated Rabi frequencies are $\Omega_{pq} = 2\pi\Delta f(\alpha E_J/\hbar) \times \langle p|\sin(2\pi f + 2\phi_m)|q\rangle$; numerical simulations of the matrix elements are consistent with recent experimental results [see caption Fig. 1(c)] [12,13,18]. A qubit initially in $|1\rangle$ can be prepared in a superposition state $|\Psi\rangle = c_1|1\rangle + c_2|2\rangle$ by temporarily driving the Ω_{12} field. Applying the Ω_{13} (Ω_{23}) field then allows the population of state $|1\rangle$ ($|2\rangle$) to be read out through a transition to state $|3\rangle$ followed by a rapid escape to the right well (a readout scheme also utilized by single-junction qubits [7]).

Alternatively, one may achieve S-EIT in a superconductive Λ system that is prepared in state $|\Psi\rangle$ by simultaneously applying the microwave fields Ω_{13} and Ω_{23} such that

$$\frac{\Omega_{13}}{\Omega_{23}} = -\frac{c_2}{c_1}. \quad (3)$$

Under this condition (with $\Omega_{12} = 0$), the state $|\Psi\rangle$ is an eigenstate of $\mathcal{H}_{\mathrm{int}}^{(\mathrm{RWA})}$ in Eq. (2) with eigenvalue zero; in this "dark state," the SQC becomes transparent to the microwave fields. As in conventional EIT, the amplitudes for the two absorptive transitions into $|3\rangle$ have equal and opposite probability amplitudes, leading to a destructive quantum interference and no population loss through the readout state $|3\rangle$. Thus, S-EIT provides a means to confirm, without disturbing the system, that one had indeed prepared the qubit in the desired state.

In a practical SQC, there will be imperfect preparation as well as decoherence of the state $|\Psi\rangle$, and this must be measured, characterized, and minimized for quantum information applications. S-EIT is a sensitive probe for this purpose, since deviations in the amplitude and/or relative phase of the complex coefficients c_i from the condition established in Eq. (3) result in a small probability $|(c_1\Omega_{13} + c_2\Omega_{23})/\Omega|^2$ (where $\Omega \equiv \sqrt{|\Omega_{13}|^2 + |\Omega_{23}|^2}$) of the SQC being driven into the readout state $|3\rangle$ on a time scale $\sim\Gamma_3/\Omega^2$. In general, there are two categories of decoherence: *loss* and *dephasing*. Loss refers to population losses from the metastable states $|1\rangle$ and $|2\rangle$, and it is present in an SQC due to both intrawell and interwell energy relaxation. Dephasing refers to interactions of the SQC with other degrees of freedom in the system that cause the relative phase between c_1 and c_2 to diffuse. Both types of decoherence act to drive even a perfectly prepared state $|\Psi\rangle$ out of the dark state defined by Eq. (3).

We describe the system with a 3×3 density matrix, where the diagonal elements ρ_{ii} describe the populations,

and ρ_{ij}, $i \neq j$ describe the coherences between levels. In the presence of the EIT fields Ω_{13} and Ω_{23} (with $\Omega_{12} = 0$), the Bloch equations govern the evolution of the density matrix [24]:

$$\dot{\rho}_{11} = -\Gamma_1\rho_{11} - \frac{i}{2}\Omega_{13}^*\rho_{31} + \frac{i}{2}\Omega_{13}\rho_{13}, \quad (4)$$

$$\dot{\rho}_{22} = -\Gamma_2\rho_{22} - \frac{i}{2}\Omega_{23}^*\rho_{32} + \frac{i}{2}\Omega_{23}\rho_{23}, \quad (5)$$

$$\dot{\rho}_{33} = -\Gamma_3\rho_{33} + \frac{i}{2}\Omega_{13}^*\rho_{31} - \frac{i}{2}\Omega_{13}\rho_{13} + \frac{i}{2}\Omega_{23}^*\rho_{32} - \frac{i}{2}\Omega_{23}\rho_{23}, \quad (6)$$

$$\dot{\rho}_{12} = -\gamma_{12}\rho_{12} - \frac{i}{2}\Omega_{13}^*\rho_{32} + \frac{i}{2}\Omega_{23}\rho_{13}, \quad (7)$$

$$\dot{\rho}_{13} = -\gamma_{13}\rho_{13} + \frac{i}{2}\Omega_{13}^*(\rho_{11} - \rho_{33}) + \frac{i}{2}\Omega_{23}^*\rho_{12}, \quad (8)$$

$$\dot{\rho}_{23} = -\gamma_{23}\rho_{23} + \frac{i}{2}\Omega_{23}^*(\rho_{22} - \rho_{33}) + \frac{i}{2}\Omega_{13}^*\rho_{21}. \quad (9)$$

The remaining three elements' equations are determined by $\rho_{ij}^* = \rho_{ji}$. The decoherence rates $\gamma_{ij} = (\Gamma_i + \Gamma_j)/2 + \gamma_{ij}^{(\mathrm{deph})}$ include both loss and dephasing contributions. We concentrate on the regime in which the readout state escape rate $\Gamma_3 = (1\ \mathrm{ns})^{-1} = (2\pi)\ 130$ MHz dominates all other loss and dephasing rates; thus $\gamma_{13} \approx \gamma_{23} \approx \Gamma_3/2$. Furthermore, we assume the dephasing rate $\gamma_{12}^{(\mathrm{deph})}$ dominates metastable state losses Γ_1 and Γ_2, setting $\Gamma_1 = \Gamma_2 = 0$ and $\gamma_{12} \approx \gamma_{12}^{(\mathrm{deph})}$. Theoretical estimates of dephasing rates, such as $\gamma_{12}^{(\mathrm{deph})}$, in multilevel systems were recently obtained in Ref. [26].

We illustrate an S-EIT decoherence probe example by applying EIT fields $\Omega_{13} = \Omega_{23} = (2\pi)$ 150 MHz to the dark state $|\Psi\rangle = (|1\rangle - |2\rangle)/\sqrt{2}$ and numerically integrating Eqs. (4)–(9). With $\gamma_{12} = 0$ the system is stationary and no population is driven into $|3\rangle$ ($\rho_{33} = 0$); when we include a dephasing rate $\gamma_{12} = (2\pi)$ 5 MHz, ρ_{33} is small but nonzero [Fig. 2(a)]. It exhibits a rapid initial rise with transitory oscillations [see inset Fig. 2(a)], reaching its maximum value $\rho_{33}^{(\mathrm{max})}$ within about $T_{\mathrm{ss}} = 4$ ns. This is followed by a smooth decay with a $1/e$ time of about 80 ns. The solid curve in Fig. 2(b) traces the total population $P = \rho_{11} + \rho_{22} + \rho_{33}$ remaining in the system as a function of time. When the excited state maximum $\rho_{33}^{(\mathrm{max})}$ is reached, the total remaining population is $P(T_{\mathrm{ss}}) = 0.973$. In contrast, the dashed line in Fig. 2(b) illustrates the rapid population loss expected when the same fields are applied to the state $|\Psi\rangle = (|1\rangle + |2\rangle)/\sqrt{2}$ [π out of phase with the dark state in Eq. (3)]. In the absence of S-EIT quantum interference, the entire population is lost on a time scale $\sim\Gamma_3/\Omega^2 \approx 4$ ns.

We now use Eqs. (4)–(9) to show how measuring the slow population loss in S-EIT can be used to extract the decoherence rate γ_{12}. The elements ρ_{33}, ρ_{13}, and ρ_{23} in

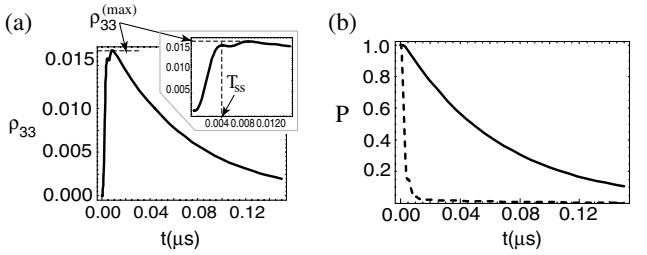

FIG. 2. (a) Population ρ_{33} versus time with EIT fields $\Omega_{13} = \Omega_{23} = (2\pi)$ 150 MHz, an initial dark state $\rho_{11} = \rho_{22} = 0.5$ and $\rho_{12} = -0.5$, and with a dephasing rate $\gamma_{12} = (2\pi)$ 5 MHz. The inset shows ρ_{33} for early times. ρ_{33} exhibits a rapid rise to a plateau after a short time T_{ss}, followed by a much slower decay. (b) The total population P remaining in the system versus time for the same simulation (solid curve). The dashed curve shows the population for the out-of-phase case $\rho_{11} = \rho_{22} = 0.5$ and $\rho_{12} = 0.5$ discussed in the text.

Eqs. (6), (8), and (9) are damped at a rapid rate $\sim\Gamma_3$, allowing their adiabatic elimination [25,27]; we solve for their quasisteady state values by setting $\dot{\rho}_{33} = \dot{\rho}_{13} = \dot{\rho}_{23} = 0$. This approximation is accurate once initial transients have passed and the plateau value $\rho_{33}^{(\mathrm{max})}$ has been reached. Using these results in Eq. (7) yields an equation for $\dot{\rho}_{12}$ with a strong damping term Ω^2/Γ_3, and it too can be solved for its quasisteady state value. In the limit $\gamma_{12}\Gamma_3/\Omega^2 \ll 1$ we obtain

$$\rho_{12}(t) \approx -\frac{\Omega_{13}\Omega_{23}}{\Omega^2}\left(1 - \frac{2\gamma_{12}\Gamma_3}{\Omega^2}\right)[\rho_{11}(t) + \rho_{22}(t)]. \quad (10)$$

The ratio $2\gamma_{12}\Gamma_3/\Omega^2$ represents the small fractional deviation of ρ_{12} from its dark state value. There is a competition between the "preparation rate" Ω^2/Γ_3 (which constantly acts to drive the system into the dark state) and the decoherence rate γ_{12} (which attempts to drive it back out).

Plugging our adiabatic solutions for ρ_{13}, ρ_{23}, and Eq. (10) into Eqs. (4) and (5) reveals that deviations from the dark state cause a loss of the population P at a rate $R = 2\gamma_{12}(\Omega_{13}^2\Omega_{23}^2/\Omega^4)P$. Since we assumed all population is lost through $|3\rangle$ via the decay term $\rho_{33}\Gamma_3$ in Eq. (6), we can equate these two rates. When the maximum $\rho_{33}^{(\mathrm{max})}$ is reached sufficiently fast, the population P is still approximately unity and this yields

$$\rho_{33}^{(\mathrm{max})} \approx 2\frac{\Omega_{13}^2\Omega_{23}^2}{\Omega^4}\frac{\gamma_{12}}{\Gamma_3}. \quad (11)$$

So long as the loss during the initial transient time $t < T_{\mathrm{ss}}$ is negligible, the population will follow a simple exponential decay $P(t) = \exp(-\rho_{33}^{(\mathrm{max})}\Gamma_3 t)$ [as in Fig. 2(b)], and the dephasing rate γ_{12} can be easily extracted. The time T_{ss} is generally the greater of the preparation time $\sim\Gamma_3/\Omega^2$ and the inverse of the decay rate $1/\Gamma_3$; the loss up to $t = T_{\mathrm{ss}}$ will be $\sim\rho_{33}^{(\mathrm{max})}\Gamma_3 T_{\mathrm{ss}} \sim (2\Omega_{13}^2\Omega_{23}^2/\Omega^4)\max(\gamma_{12}/\Gamma_3, \gamma_{12}\Gamma_3/\Omega^2)$, requiring both ratios in the max$(\cdots)$ argument to be small. The first ratio

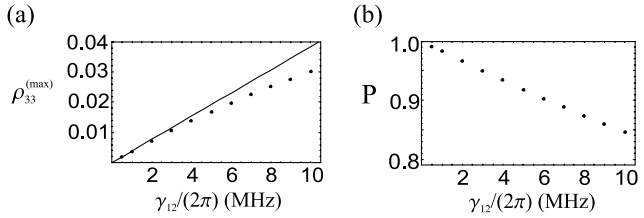

FIG. 3. (a) The maximum plateau value $\rho_{33}^{(max)}$ for different γ_{12} (circles). The solid curve shows the prediction (11). (b) The remaining population $P = \rho_{11} + \rho_{22} + \rho_{33}$ at the time the plateau is reached T_{ss} for the cases in (a).

will generally be small for parameters of interest while the second can be made small by choosing an appropriate field strength Ω. When these conditions are satisfied, the method outlined here can be used to measure γ_{12}. Note also that if one applies the S-EIT fields for a time $T_{\text{S-EIT}} \gg T_{ss}$ and observes no loss, then the prepared superposition $|\Psi\rangle$ is unperturbed and one has still obtained an upper bound on the decoherence rate γ_{12}.

We have performed a series of numerical simulations, varying γ_{12}, to validate the preceding approach. Figure 3(a) indicates $\rho_{33}^{(max)}$ versus γ_{12} and compares the numerical results with the analytic estimate [Eq. (11)]. The agreement is good for $\gamma_{12} < (2\pi)4$ MHz, which corresponds to $2\gamma_{12}\Gamma_3/\Omega^2 < 0.056$. Higher dephasing rates compete more with the preparation rate, making the adiabatic elimination approach used to obtain Eqs. (10) and (11) less valid. In such cases, one observes a significant loss of P by the time $\rho_{33}^{(max)}$ is reached, as illustrated in Fig. 3(b).

In employing the RWA in Eqs. (4)–(9), we have ignored the field-induced couplings of far off-resonant transitions, which can drive the system out of the dark state [e.g., in Fig. 1(c): although detuned by $|\Delta| \approx 4$ GHz, Ω_{23} weakly drives $|1\rangle \leftrightarrow |2\rangle$]. We have performed calculations of the evolution including all such couplings for our parameters and found they induce an additional absorption into $|3\rangle$ at a rate $R_{\text{off-res}} = (2\pi)$ 19 kHz. Such transitions will not effect our S-EIT measurement for qubit decoherence rates $\gamma_{12} \gg R_{\text{off-res}}$. The effect is analogous to ac Stark shifts and Rayleigh scattering in atoms [28], and it has been shown [25] that the loss rate scales as $R_{\text{off-res}} \sim \Gamma_3(\Omega^2/\Delta^2)$, $\Omega^4/\Gamma_3\Delta^2$, which introduces a maximum allowed field intensity Ω^2 for a given detuning Δ and decoherence rate γ_{12}.

We have proposed using the superconductive analog to EIT (S-EIT) to demonstrate macroscopic quantum interference in superconductive quantum circuits. We have shown how S-EIT can be used to measure, with a single pulse of the two S-EIT fields, whether a particular superposition of metastable energy levels (a qubit) has been prepared. The technique is distinguishable from previous state measurement schemes [7] in that S-EIT ideally does not disturb the system, preserving its quantum coherence when it has been prepared in the desired state. Furthermore, we have shown how S-EIT can very sensitively probe small qubit errors due to decoherence or imperfect state preparation, and we have obtained analytic expressions for the field strengths required to measure the qubit dephasing rate.

This work was supported in part by AFOSR Grant No. F49620-01-1-0457 under the Department of Defense University Research Initiative in Nanotechnology (DURINT) and by AFOSR Grant No. FA-9550-04-1-0221. The work at Lincoln Laboratory was sponsored by the AFOSR under Air Force Contract No. F19628-00-C-0002.

[1] A. J. Leggett and A. Garg, Phys. Rev. Lett. **54**, 857 (1985).
[2] Y. Nakamura, Y. A. Pashkin, and J. S. Tsai, Nature (London) **398**, 786 (1999); Y. A. Pashkin *et al.*, *ibid.* **421**, 823 (2003).
[3] J. R. Friedman *et al.*, Nature (London) **406**, 43 (2000).
[4] C. H. van der Wal *et al.*, Science **290**, 773 (2000).
[5] D. Vion *et al.*, Science **296**, 886 (2002).
[6] Y. Yu *et al.*, Science **296**, 889 (2002).
[7] J. M. Martinis, S. Nam, J. Aumentado, and C. Urbina, Phys. Rev. Lett. **89**, 117901 (2002).
[8] I. Chiorescu *et al.*, Science **299**, 1869 (2003).
[9] K. J. Boller, A. Imamoglu, and S. E. Harris, Phys. Rev. Lett. **66**, 2593 (1991).
[10] S. E. Harris, Phys. Today **50**, No. 7, 36 (1997).
[11] J. Ruostekoski and D. F. Walls, Phys. Rev. A **59**, R2571 (1999).
[12] Y. Yu *et al.*, Phys. Rev. Lett. **92**, 117904 (2004).
[13] D. S. Crankshaw *et al.*, Phys. Rev. B **69**, 144518 (2004).
[14] T. P. Orlando *et al.*, Phys. Rev. B **60**, 15 398 (1999).
[15] L. V. Hau, S. E. Harris, Z. Dutton, and C. H. Behroozi, Nature (London) **397**, 594 (1999).
[16] M. M. Kash *et al.*, Phys. Rev. Lett. **82**, 5229 (1999).
[17] D. Budker, D. F. Kimball, S. M. Rochester, and V. V. Yashchuk, Phys. Rev. Lett. **83**, 1767 (1999).
[18] K. Segall *et al.*, Phys. Rev. B **67**, 220506 (2003).
[19] Z. Zhou, S.-I. Chu, and S. Han, Phys. Rev. B **66**, 054527 (2002); C.-P. Yang, S.-I. Chu, and S. Han, Phys. Rev. A **67**, 042311 (2003).
[20] M. H. S. Amin, A. Yu. Smirnov, and A. Maasen van den Brink, Phys. Rev. B **67**, 100508(R) (2003).
[21] Z. Kis and E. Paspalakis, Phys. Rev. B **69**, 024510 (2004).
[22] J. E. Mooij *et al.*, Science **285**, 1036 (1999).
[23] D. Nakada *et al.* (to be published).
[24] M. O. Scully and M. S. Zubairy, *Quantum Optics* (Cambridge University Press, Cambridge, 1997).
[25] Z. Dutton, Ph.D. thesis, Harvard University, 2002.
[26] G. Burkard, R. H. Koch, and D. P. DiVincenzo, Phys. Rev. B **69**, 064503 (2004).
[27] J. Javanainen and J. Ruostekoski, Phys. Rev. A **52**, 3033 (1995).
[28] C. Cohen-Tannoudji, J. Dupont-Roc, and G. Grynberg, *Atom-Photon Interactions* (John Wiley & Sons, Inc., New York, 1992).